Magnetic guide for neutral atoms

James A. Richmond, Benjamin P. Cantwell, Síle Nic Chormaic,* David C. Lau,† Alexander M. Akulshin, and Geoffrey I. Opat
School of Physics, The University of Melbourne, Victoria 3010, Australia
(Received 18 July 2001; published 1 March 2002)

A solenoid consisting of two interwound helical coils carrying equal but opposite currents can act as a guide for neutral atoms. In this paper we develop the theory of such a guide and report on its performance in guiding laser-cooled cesium atoms. Our guide is a useful tool for transporting cooled atoms since it prevents ballistic expansion of the atomic cloud after it is released from a magneto-optical trap. In contrast to atom-guide designs using permanent magnets, our guide can be switched off by switching the currents; hence it can be placed close to a magnetic trap without adversely affecting the trapping efficiency. One of the unique features of this guide is that, except in the immediate neighborhood of the walls of the guide, the atoms are not magnetically perturbed to any appreciable extent by the guide field. This opens up the possibility of a system for cooling atoms.

DOI: 10.1103/PhysRevA.65.033422 PACS number(s): 03.75.Be, 32.80.Pj, 03.75.−b

I. INTRODUCTION

With the development of magneto-optical techniques for cooling and trapping neutral atoms [1,2], interest has grown in the parallel development of optical elements for manipulating cold atoms, including atomic mirrors, diffraction gratings, and beam splitters. These elements are required for the realization of atom interferometers with large enclosed areas. Such interferometers will be extremely sensitive to inertial and rotational effects [3], permitting accurate measurements of fundamental constants and atomic properties.

There is a need for efficient adiabatic transport mechanisms for cold atoms, Bose-Einstein condensates [4,5], and beams derived from them [6–9]. A number of atom-guide configurations have recently been demonstrated, which can be conveniently categorized as either optical guides or magnetic guides.

Optical guides rely on the dynamic electric-dipole interaction between neutral atoms and laser light. Atoms in light fields experience an energy shift, which gives rise to an optical dipole potential and hence a force [10,11]. If the laser frequency is set slightly lower than an atomic resonance (''red detuning'') atoms are attracted to high-intensity regions; if slightly above a resonance (''blue detuning'') atoms are repelled from these regions. The detuning from resonance is usually chosen to be relatively large in order to avoid unwanted spontaneous scattering.

Optical guiding has been demonstrated in both hollow optical fibers and laser beams. Many recent fiber guides have used hollow-core optical fibers in which a blue-detuned laser is injected into the annular region of a fiber at grazing incidence [12–14]. Low-velocity atoms injected into the central region are repelled by the evanescent wave created by the light field at the inner surface of the hollow region. Other hollow fiber guides have employed red-detuned laser light injected into the hollow region [15].

Several optical guides consisting of ''hollow'' laser beams have been demonstated [16–21]. A common configuration uses a blue-detuned Laguerre-Gaussian beam, in which atoms are repelled from high-intensity regions and guided along a ''dark'' axis of the beam. All-light guides generated using microfabricated optical elements appear to provide a very promising new approach to manipulating atoms using optical dipole forces [22,23].

Magnetic guides for neutral atoms use the interaction between an atom's intrinsic magnetic dipole moment and an external magnetic field to guide atoms, as described in the following section. A valuable recent review of experiments in magnetic atom optics, which includes a discussion of guides, was written by Hinds and Hughes [24].

One approach to making magnetic guides for neutral atoms has involved arrangements of permanent magnets (most often rare-earth materials) [25,26]. Permanent magnet guides have some advantages over other magnetic guides. However, the fact that they cannot be switched off when not required can be disadvantageous in many applications. For this reason, most magnetic guides are based on current-carrying structures.

There have been several recent demonstrations of atom guiding using current-carrying wires close to a magneto-optical trap (MOT). Guiding has been demonstrated around a single wire [27] and near an arrangement of two wires attached to each other [28]. Arrangements of four wires to form a magnetic-quadrupole guide have been demonstrated both with free-standing wires in which the axis of the guide intersects the center of a magneto-optical trap [29] and with miniature wires embedded in a silica fiber [30]. Other configurations have been proposed [31–33].

Like optical guides, microfabrication of current-carrying structures on substrates appears to be a promising approach to the magnetic manipulation of cold atoms [34]. Previously, loading of atoms from a MOT into guides formed by currents on such substrates has been a challenge, but solutions such as the ''mirror MOT'' [35,36] are continually being found. Sev-

*Present address: Department of Applied Physics and Instrumentation, Cork Institute of Technology, Cork, Ireland.
†Present address: SCOAP, CPES, University of Sussex, Falmer, Brighton BN1 9QH, UK.

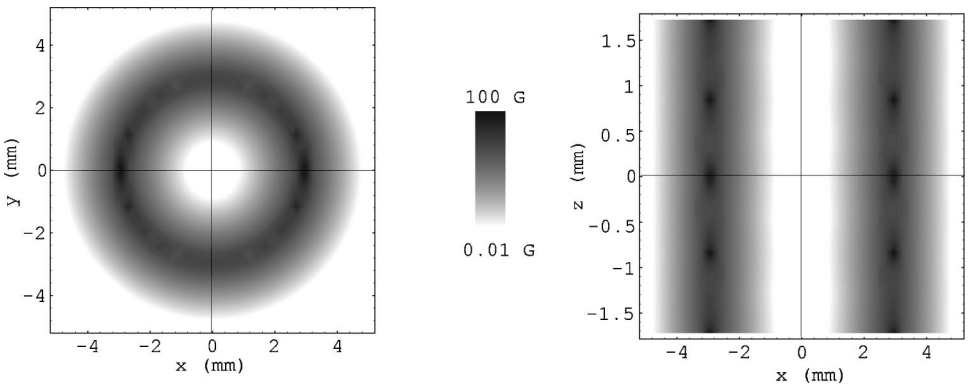

FIG. 1. Magnetic-field magnitude of a double-wound solenoid with $R=2.93$ mm, $a=1.72$ mm carrying a current of 1 A. Darker regions on the plots represent higher field magnitudes. The (x,y) plot is for the plane $z=0$. The solenoid wires intersect this plane at $(x=\pm R, y=0)$. The (x,z) plot is for the plane $y=0$. Note that the magnitude scale is logarithmic.

eral ''atom chips'' of this type have been demonstrated [37–41].

We have constructed and tested a magnetic guide consisting of two identical interwound helical solenoids. Adjacent wires carry equal but opposite currents. This guide shares the advantages of other current-carrying guides in that it can be switched on and off as required. Another feature of this guide is that, except in the immediate neighborhood of the walls of the guide, the atoms are not magnetically perturbed to any appreciable extent by the guide field. In contrast to the wire and microfabricated guides discussed above, our guide has a large volume in which the atoms experience essentially no magnetic field (apart from any additional bias field applied in order to prevent unwanted spin flips, as described below). This opens up the possibility of a system for cooling atoms, as discussed at the end of this paper.

II. MAGNETIC GUIDING OF NEUTRAL ATOMS

The permanent magnetic-dipole moment $\boldsymbol{\mu}$ of a neutral atom in an inhomogeneous magnetic field $\boldsymbol{B}$ has a potential energy given by

$$U=-\boldsymbol{\mu}\cdot\boldsymbol{B}=gm_F\mu_B|\boldsymbol{B}(\boldsymbol{r})|,$$

where g is the atomic Landé factor, m_F is the azimuthal quantum number, and μ_B is the Bohr magneton. The atom experiences a position-dependent force

$$\boldsymbol{F}=-\boldsymbol{\nabla}U=-gm_F\mu_B\boldsymbol{\nabla}|\boldsymbol{B}(\boldsymbol{r})|.$$

When $gm_F>0$, the force pushes the atom away from regions with high magnetic-field magnitudes towards regions of lower field and lower potential energy. Provided that the rate of change of the field direction with time (as seen by the moving atom) is small compared with the Larmor-precession frequency, the projection of the atomic dipole moment onto the local field direction remains constant throughout the motion (i.e., m_F does not change). This adiabatic condition was satisfied in the experiments discussed below.

III. THE SOLENOID MAGNETIC GUIDE

Every undergraduate has calculated the field of an infinitely long helical solenoid using Ampère's circuital law [42]. The solution obtained this way is only an approximation, as it ignores the axial component of the current and the periodicity of the windings.

A *double-wound* solenoid consists of two interwound helical coils of wire. If the wires carry equal and opposite currents the undergraduate calculation tells us the magnetic field is exactly zero inside and outside the solenoid. This solution is incorrect near the windings, where there is in fact a sizeable, spatially periodic field.

An exact calculation of the magnetic fields of single- and double-wound solenoids is given in the Appendix. Inside the double-wound solenoid the field magnitude decreases exponentially from the walls. The central region of the guide is essentially field-free, which means that undesirable Zeeman shifts are avoided. The calculated field magnitude of our experimental double-wound guide is shown in Fig. 1.

IV. EXPERIMENTAL METHOD

We tested our guide using cesium atoms laser cooled in a magneto-optical trap.

A. The guide

Our test guide consisted of two interwound solenoids made from Kapton-coated wire of diameter 0.86 mm. The two solenoids were wound as tightly as possible using this wire, giving a periodicity between adjacent turns on each separate wire of twice the wire diameter (i.e., $a=1.72$ mm). The wires were wound around a cylindrical rod of radius 2.5 mm, which was then removed, resulting in a guide radius of $R=2.93$ mm [33].

The total length of the guide was 38 mm, limited by the dimensions of our vacuum chamber and the space available for the trapping and other laser beams (see below). The wire solenoids were supported by a mount external to the windings. The guide was mounted vertically in the vacuum chamber, 15 mm below the MOT.

B. Trapping and cooling of cesium atoms

Our MOT consisted of three pairs of mutually orthogonal laser beams of diameter ~ 2 cm and power ~ 5 mW, intersecting at the center of a magnetic field produced by a set of coils in an anti-Helmholtz configuration. Each beam consisted of a superposition of light from two diode lasers—a trapping and a repumping laser. The trapping laser was

locked to the $6\ ^2S_{1/2}(F=4)\rightarrow 6\ ^2P_{3/2}(F=5)$ resonance of cesium, while the repumping laser was locked to the $6\ ^2S_{1/2}(F=3)\rightarrow 6\ ^2P_{3/2}(F=4)$ transition. Each pair of beams was counter propagating in a σ^+/σ^- configuration. The combination of the inhomogeneous magnetic field produced by the coils and the laser light had the effect of confining atoms in the intersection region of the beams. The repumping light prevented the loss of cesium atoms from the trapping light field.

The MOT was located in a vacuum chamber with a base vapor pressure less than 10^{-8} Torr. Caesium atoms were trapped and cooled in the MOT in a two-step process. First, the trap was loaded for 3.6 sec from the background cesium vapor in the chamber, with the trapping lasers red detuned by about 10 MHz from the locked frequency (corresponding to approximately two natural linewidths). The coils providing the trapping magnetic field were then switched off and the atoms were further cooled in optical molasses for 20 ms, with the trapping lasers detuned by an additional 40 MHz. This typically resulted in the capture and cooling of around 10^7 atoms with a final temperature of approximately 20 μK, measured using a time-of-flight technique.

C. Experimental arrangement

After cooling, the atoms were released from the trap by blocking the trapping laser beams. The atomic cloud fell towards the guide, expanding ballistically due to the small residual velocities of the atoms.

Optionally, at a distance of about 1 cm below the trap, the atoms could be optically pumped into particular hyperfine substates of the cesium $F=4$ ground level. The optical pumping beam consisted of light from a diode laser tuned to the cesium $6\ ^2S_{1/2}(F=4)\rightarrow 6\ ^2P_{3/2}(F=4)$ transition, superposed with light from the repumping laser described above. The beam had a horizontal width equal to the diameter of the guide, a vertical height of approximately 1 mm, and a power of around 1 μW. The light was retroreflected to minimize any net transfer of momentum from this beam to the falling atoms. Due to constraints imposed by the positioning of the trapping beams, the optical pumping beam was inclined at about 10° to the horizontal.

A small horizontal magnetic field ($\approx$0.5 G) approximately parallel to the pump and probe beams (see below) was switched on 1 ms after the atoms were released from the trap. A bias field of this type is necessary to prevent atoms inside the guide from experiencing Majorana spin flips, which might occur in the otherwise low field in the interior of the guide. The direction of the field chosen here also fixed an appropriate quantization direction for the atoms relative to the pump and probe beams.

Given the relatively large periodicity of the guide's windings in this experiment, the rate of change of the magnetic-field direction, as experienced by atoms falling through the guide, was calculated to be always much smaller than their Larmor-precession frequency. The motion was therefore adiabatic in that the atoms maintained a constant magnetic quantum number (m_F) throughout the experiment.

After falling through the guide, the atoms passed through a 1-μW/cm^2 probe laser beam of the same dimensions as the pump beam. The probe beam, resonant with the $6\ ^2S_{1/2}(F=4)\rightarrow 6\ ^2P_{3/2}(F=5)$ transition, was positioned 2 mm below the lower end of the guide. The intensity of this beam after passing below the guide was measured by focusing it onto a photodiode. When atoms fell through the beam, some of the probe light was absorbed, resulting in a measurable decrease in intensity.

Measurements of the probe intensity were made continuously for many trap cycles (consisting of trapping and releasing atoms, then waiting for them to fall through the probe beam). The guide was switched on in alternate trap cycles. The absorption of the probe light was expected to be directly proportional to the number of atoms falling through the probe beam. The ratio of the number of atoms passing through the beam when the guide was switched on to when no current flowed was then equal to the ratio of the measured beam intensities in alternate trap cycles.

D. Monte-Carlo simulation

A computer program was written to simulate the behavior of atoms in the guide. Atoms were given random positions and velocities in the simulated trap, the velocities being selected according to a Maxwell-Boltzmann distribution based on the measured average temperature of atoms in the trap (20 μK). The trajectory of each atom was then calculated. Some atoms did not enter the guide. Others fell straight through the guide without interacting significantly with the magnetic field. Some atoms were reflected by the guide walls.

The trajectories of atoms in a long guide of this type are generally complicated, particularly where the atoms are initially displaced from the center of the trap. However, given the dimensions of our test guide it can be shown that most atoms interacting with the guide walls experience only one reflection before exiting at the lower end of the guide.

The expected fractional increase in the absorption of the probe light is

$$f=(s+r)/s,$$

where s is the number of atoms falling straight through the guide and r is the number of atoms reflected by the guide walls.

The guide was initially modeled as having ''hard'' walls at a distance of 2.5 mm from the guide center. Later simulations included a more accurate calculation of the radial distance at which each atom would be reflected, based on the current in the guide and the magnetic substate of each atom.

V. EXPERIMENTAL RESULTS

A. Varying switch-on time

The absorption of the probe light was measured as a function of the time at which the guide was switched on. The results are shown in Fig. 2. For this experiment, the atoms were optically pumped towards magnetic substates with $m_F>0$.

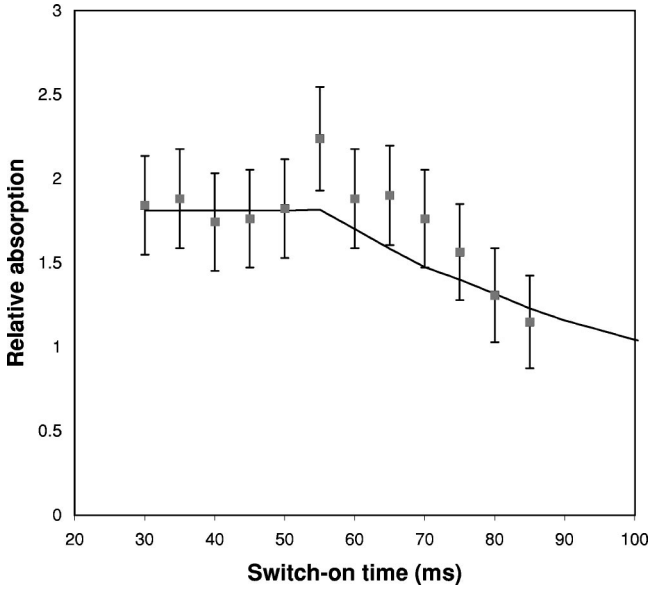

FIG. 2. Measured absorption of probe light as a function of the tube switch-on time. The solid line shows the absorption predicted by the Monte Carlo simulation.

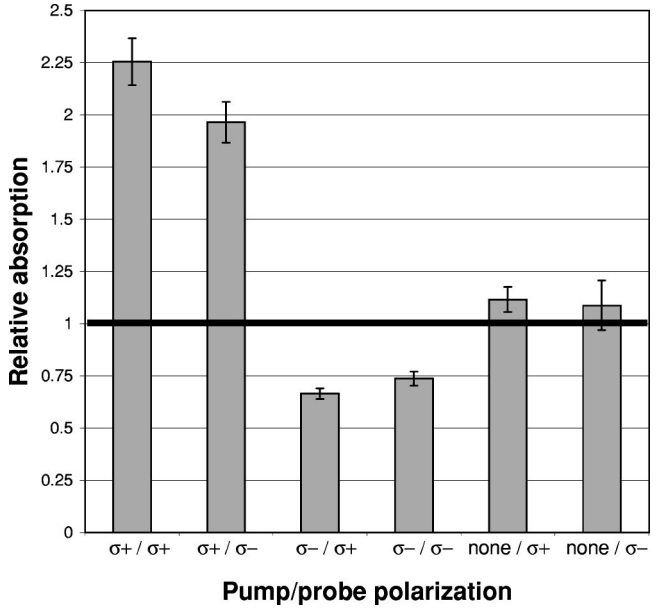

FIG. 3. Measured absorption of the probe light as a function of polarization of the optical pumping and probe beams. An increase in absorption is seen with σ^+ pumping, which puts atoms into states that are reflected by the guide. A corresponding decrease is seen with σ^- pumping.

The horizontal axis shows the time delay between releasing the atoms from the trap and switching on the current in the guide. The vertical axis shows the ratio of the absorption when the guide was switched on during a trap cycle to the absorption when the guide remained off. For this experiment, a current of 1.00 A was used in both the windings. Theoretical calculations show that this current is sufficient for the guide to confine the majority of atoms in positive magnetic substates ($m_F>0$) at the average trap temperature. The atoms were optically pumped using σ^+ light.

A simple time-of-flight calculation shows that atoms free falling from rest at the center of the trap take 55 ms to reach the top of the guide, and 104 ms to reach the lower end. The experimental results show a clear decrease in the number of atoms passing through the probe beam as the guide is switched on at later times. This is due to the reduction in the effective reflecting length of the guide as the switch-on time is varied. Due to the geometry of the experiment and the temperature of the atoms, little difference is seen in absorption for switch-on times later than 85 ms, even though with this switch-on time approximately half the guide is still available to reflect atoms.

The solid line shows the expected absorption ratio as predicted by the Monte Carlo simulation. In general, the measured increase in absorption was a little larger than expected. The particularly large increase at the switch-on time of 55 ms could be due to fringe magnetic fields at the top end of the guide having an additional guiding effect on those atoms reaching the entrance earlier or later than average due to their initial velocities.

The calculated errors were obtained by examining the variation in the measured absorption between consecutive pairs of trap cycles, both with the guide current on and off. This variation was probably due mainly to fluctuations in the total number of atoms trapped in each cycle. Possibly, small instabilities in the gain of the amplifier used to measure the absorption of the probe light also contributed to the variation.

B. Varying polarization of pump and probe beams

For this part of the experiment, the guide was switched on 55 ms after the atoms were released from the trap (i.e., as the atoms falling from rest at the trap center reached the top of the guide). The current, again 1.00 A in each winding, remained on until long after the atoms had fallen through the probe beam.

Atoms were optically pumped by the pump beam described above. Absorption measurements were made for atoms pumped with circularly polarized (σ^+ or σ^-) light and compared with the case where there was no optical pumping. The polarization of the probe laser was similarly varied. Some typical results are shown in Fig. 3.

With σ^+ pumping, we observed an increase in the number of atoms passing through the probe beam. This pumping puts most of the atoms into magnetic states with $m_F>0$. For the cesium $F=4$ ground level, these states are repelled from the walls of the guide. Some atoms, which would have hit the guide walls if no current was flowing, are instead reflected one or more times, eventually passing through the probe beam.

With σ^- pumping, on the other hand, we observed a decrease in the number of atoms falling through the probe beam. With this polarization, most of the atoms are pumped to states with $m_F<0$. These atoms are attracted to the walls of the guide, leading to a greater loss of atoms than when there is no current.

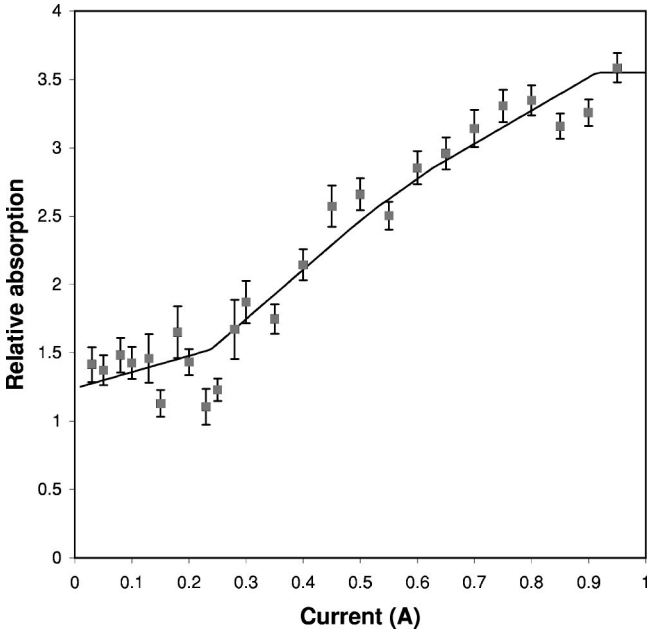

FIG. 4. Measured absorption of the probe light as a function of the guide current. The solid line is a linear model fitted to the experimental data (as described in the text). The observed absorption increases with increasing current in the guide.

The experimental results agree reasonably well with the predictions of the Monte Carlo simulation. The switch-on time of 55 ms could account for the slightly larger than expected increase in absorption with σ^+ pumping. The observed decrease in absorption with σ^- pumping was well predicted by the simulation. In calculating the guide's behavior for the σ^- case, we assumed that all the atoms in substates with $m_F<0$, which would have been reflected by the guide walls in the corresponding $m_F>0$ substate, were effectively absorbed by the walls of the guide (e.g., by sticking to the walls).

With no optical pumping, some of the $m_F>0$ atoms were reflected by the guide, while some of the atoms with $m_F\leqslant 0$ were attracted to the walls. The combination of these two effects led us to expect a small net increase in absorption when the guide was switched on. This is seen in the experimental results.

Variations in the polarization of the probe laser had little effect on the measured absorption, most likely due to the relatively long interaction times between the atoms and the probe light.

C. Varying current

As in the previous experiment, the current was switched on as atoms reached the top of the guide, and remained on until after the atoms had fallen through the probe beam. The current in the windings was varied from zero to 1.00 A. The atoms were not optically pumped.

Some typical results are shown in Fig. 4. As the current was increased, more atoms were reflected by the walls of the guide, leading to increased absorption of the probe light.

Initially, when the results of Fig. 4 were compared to results from the Monte Carlo simulations, the experimental behavior did not seem to match the predictions of the simulation. The theoretical curve showed a more rapid initial increase in absorption than the experimental data. However, we observed during this experiment that the trap was not well centered over the guide, but rather was offset slightly to one side. When this was taken into account, the observed behavior matched the simulation well.

This experiment was conducted without optical pumping. We, therefore, expected four magnetic substates ($m_F=+1$, $+2,+3,+4$) to contribute to the observed absorption increase as the current was varied. A linear model (the solid line on the graph) was developed and fitted to the experimental data. The free parameters for the fit were the threshold current I_0 needed to reflect atoms in the $m_F=+4$ substate, the relative populations of each substate in the atomic ensemble, and a parameter s, related to the gradients of the fitted curve sections. If we consider all the atoms with a particular (positive) value of m_F, then those atoms having zero velocity in the trap are reflected by the guide walls when the current exceeds the threshold current $4I_0/m_F$. Other atoms in the same substate are reflected at higher or lower currents. We assume a linear increase with current in the fraction of atoms reflected in each substate, the rate of which depends on the initial velocity distribution of the atoms (or equivalently the trap temperature). This rate is quantified by the parameter s.

From the fit, the threshold current for the data in Fig. 4 was $I_0=0.14$ A, which agrees well with the theoretical prediction. The relative populations of the reflected substates were, for the $m_F=+1,+2,+3,+4$ states, 67%, 15%, 10%, and 7%, respectively, indicating probable optical pumping in the trap.

We see from the plot that initially only $m_F=+4$ atoms are reflected by the guide walls. As the current is increased, the $m_F=+3$ atoms start to be reflected, followed by the $m_F=+2$ and $m_F=+1$ atoms. Clear plateaus between adjacent substates are not seen in the fitted curve, since the velocity distribution of the atoms is such that not all of the atoms in a particular substate are reflected when atoms in the next lower substate start to be reflected at a particular current.

VI. CONCLUSION AND OUTLOOK

We have constructed and tested a magnetic guide consisting of interwound wire solenoids. Our results clearly demonstrate confinement of atoms inside the guide structure. In future work, we would also like to demonstrate guiding of atoms when our guide is not vertical, as well as guiding around a bend.

The large low-field region inside our guide suggests a possible method for cooling atoms. If the currents in the two wires of our guide are not of equal magnitude, or if a constant external field is applied in addition to the guide field, this has the effect of ''roughening'' the walls of the guide. As atoms reflect from the walls, some kinetic energy can be transferred from the axial direction of the guide to the trans-

verse direction. A red-detuned, σ^+ polarized laser could be used to cool atoms in the axial direction. Alternatively, a pair of counterpropagating, red-detuned beams could be used. In contrast to the usual configuration of counterpropagating beams in a MOT, both beams passed along the guide axis would have σ^+ polarization. In either case, the combination of the guide's magnetic confinement and the cooling by the light field could result in three-dimensional cooling of atoms in the guide. A third possibility would be to confine atoms to the annular region between a blue-detuned beam (passed along the axis) and the guide walls. None of these methods would constitute a trap, since although the atoms would be confined in the guide, they would still be free to move in the axial direction.

The Zeeman splitting of the energies of different magnetic substates is insignificant in our guide since it would be small compared with the natural linewidth of the atomic transition excited by the laser. For example, for a laser tuned to the cesium $6\ ^2S_{1/2}(F=4)\rightarrow 6\ ^2P_{3/2}$ transition,

$$\frac{\Delta\omega}{\Gamma}=\frac{g\mu_B|\boldsymbol{B}|}{\hbar\Gamma}\approx 0.07|\boldsymbol{B}|,$$

where $\Delta\omega$ is the Zeeman splitting, Γ is the natural linewidth, and $|\boldsymbol{B}|$ is measured in Gauss. In comparison with a quadrupole guide in which the magnetic field increases from the axis as r^1, or a hexapole guide in which the magnetic field increases as r^2, the field of our guide falls off exponentially with distance from the wires. Thus there is a large region for which $\Delta\omega/\Gamma \ll 1$. Using the formulas in the Appendix it can be shown that at distances greater than 1.7 wire radii from the guide walls, the guide's magnetic field (capable of confining cold atoms) produces a Zeeman splitting less than 10% of the natural linewidth of the above transition. A laser would therefore interact equally with atoms in all substates.

In any arrangement for cooling atoms in the guide or for directing atoms around a bend, care would need to be taken to prevent nonadiabatic transitions of atoms into magnetic substates not confined by the magnetic dipole force. A small, constant magnetic field inside the guide would ensure that atoms would not encounter regions of negligible field. An external field similar to that used in our tests, but in the axial direction, could be used for this purpose. (Its magnitude need not be as large as was used above.) Unbalancing the currents a little in the guide windings would have the same effect. In either case, the small constant field would roughen the walls without adversely affecting their ability to confine atoms. Moreover, the statements made above regarding the Zeeman splitting of the atomic energy levels in the interior of the guide would remain valid.

With any such bias field, it would be important to ensure that any laser beams propagating along the guide axis had σ^+ polarization to avoid optical pumping into untrapped magnetic states. Because of the variability in the direction of the magnetic field in the neighborhood of the guide walls, it would be important to confine the laser light to a region near the center of the guide.

We present the cooling scheme outlined above as a tentative proposal, which will require a more detailed theoretical investigation beyond the scope of this article.

ACKNOWLEDGMENTS

The authors are indebted to Peter Hannaford, Andrei Sidorov, and Russell McLean of the CSIRO Laser Spectroscopy group. They also acknowledge the financial support of the Australian Research Council (ARC).

APPENDIX: THEORY

1. Introduction

Exact expressions for the magnetic field of a solenoid are calculated below, starting from a general expression for the current density of a wire. We also find the field of a double-wound solenoid using the derived expressions.

2. Current density of a current-carrying wire

A wire of negligible thickness carries a current I. The path and unit tangent vector of the wire are given by

$$\boldsymbol{r}=\boldsymbol{r}(s),\quad \boldsymbol{t}(s)\equiv d\boldsymbol{r}(s)/ds, \tag{A1}$$

where s is the distance along the wire from an arbitrary point.

It can be shown that the current density of the wire is given by

$$\begin{aligned}\boldsymbol{J}(\boldsymbol{r})&=\int_i^f I(s)\,\delta^3(\boldsymbol{r}-\boldsymbol{r}(s))\boldsymbol{t}(s)ds\\&=\int_i^f I(\lambda)\,\delta^3(\boldsymbol{r}-\boldsymbol{r}(\lambda))\frac{d\boldsymbol{r}(\lambda)}{d\lambda}d\lambda.\end{aligned} \tag{A2}$$

In the second expression, an arbitrary path parameter λ has been employed. $\boldsymbol{J}$ is zero except when $\boldsymbol{r}$ lies on the path of the wire, in which case it points in the direction of the tangent vector.

3. Magnetic field of a solenoid

A helical solenoid carrying current I is characterized by R, the radius of the coil, and a, the axial distance between adjacent wires. Note that a is the reciprocal of the number of turns per unit length. We treat the solenoid as infinite in length, with wires of negligible thickness.

a. Equations

The magnetic field is obtained by solving Maxwell's equations,

$$\nabla\cdot\boldsymbol{B}=0,\quad \nabla\times\boldsymbol{B}=\mu_0\boldsymbol{J}. \tag{A3}$$

Given the symmetries of the solenoid, a cylindrical coordinate system is used, as shown in Fig. 5. The path of the wire is given by

$$r=R,\quad \phi=2\pi\nu,\quad z=z_0+a\nu, \tag{A4}$$

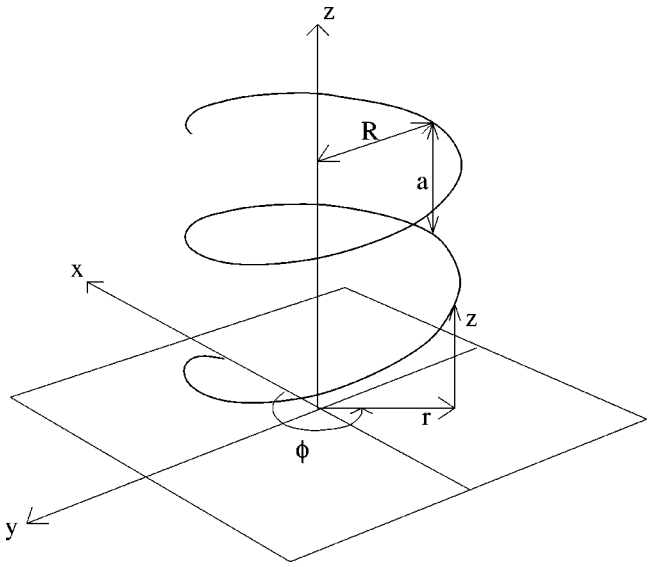

FIG. 5. Cylindrical co-ordinate system used to describe the solenoid and associated magnetic field. The solenoid is characterized by the parameters R (the radius) and a (the distance between adjacent wires in the axial direction).

where ν is a continuous parameter describing the number of turns counted from an arbitrary starting point $z=z_0$. Using Eq. (A2) with $\lambda=\nu$, we obtain

$$J_r=0, \tag{A5a}$$

$$J_\phi=\frac{I}{a}\delta(r-R)\sum_{m=-\infty}^{\infty}\delta\left(\frac{\phi}{2\pi}-\frac{z-z_0}{a}+m\right), \tag{A5b}$$

$$J_z=\frac{I}{2\pi R}\delta(r-R)\sum_{m=-\infty}^{\infty}\delta\left(\frac{\phi}{2\pi}-\frac{z-z_0}{a}+m\right). \tag{A5c}$$

To solve Eqs. (A3) we exploit the helical symmetries of the solenoid. The symmetries of any vector $\boldsymbol{V}$ associated with the solenoid (including $\boldsymbol{J}$ and $\boldsymbol{B}$) are

$$V_i(r,\phi+2\pi n,z)=V_i(r,\phi,z), \tag{A6a}$$

$$V_i(r,\phi,z+na)=V_i(r,\phi,z), \tag{A6b}$$

$$V_i(r,\phi+2\pi\nu,z+\nu a)=V_i(r,\phi,z). \tag{A6c}$$

Here, n is an arbitrary integer, ν is an arbitrary angle (in revolutions), and i denotes a cylindrical component r, ϕ, or z. Choosing $\nu=-z/a$, Eq. (A6c) becomes

$$V_i(r,\phi-2\pi z/a,0)=V_i(r,\phi,z), \tag{A7}$$

showing that the V_i are functions of only two independent variables, r and $\phi'\equiv\phi-2\pi z/a$.

Expanding V_i as a Fourier series, we obtain

$$V_i=\sum_{n=-\infty}^{\infty}v_{i,n}(r)\exp(in\phi'), \tag{A8}$$

with

$$v_{i,n}(r)=\frac{1}{2\pi}\int V_i(r,\phi')\exp(-in\phi')d\phi'. \tag{A9}$$

Since the V_i are real, the $v_{i,n}(r)$ satisfy

$$v_{i,-n}(r)=[v_{i,n}(r)]^*. \tag{A10}$$

Applying Eqs. (A4)–(A9) to Eqs. (A3), we find

$$\frac{1}{r}b_{r,n}+\frac{db_{r,n}}{dr}+\frac{in}{r}b_{\phi,n}-\frac{i2\pi n}{a}b_{z,n}=0, \tag{A11a}$$

$$b_{\phi,n}+\frac{a}{2\pi r}b_{z,n}=0 \quad (n\neq 0), \tag{A11b}$$

$$-\frac{i2\pi n}{a}b_{r,n}-\frac{db_{z,n}}{dr}=\frac{\mu_0 I}{a}\delta(r-R)\exp\left(\frac{i2\pi nz_0}{a}\right), \tag{A11c}$$

$$\frac{1}{r}b_{\phi,n}+\frac{db_{\phi,n}}{dr}-\frac{in}{r}b_{r,n}=\frac{\mu_0 I}{2\pi R}\delta(r-R)\exp\left(\frac{i2\pi nz_0}{a}\right). \tag{A11d}$$

For each order n, the equations are decoupled. Further, except at $r=R$, the right-hand sides of all these equations are zero. Since we require $\boldsymbol{B}$ to be finite at $r=0$ and zero as $r\to\infty$ the $b_{i,n}$ also satisfy these conditions. We also note that $b_{\phi,n}$ and $b_{z,n}$ are discontinuous across $r=R$.

b. Solution for n=0

Solving Eqs. (A11a), (A11c), and (A11d) for $n=0$ gives

$$B_r=0, \tag{A12a}$$

$$B_\phi=\begin{cases}\mu_0 I/(2\pi r) & \text{if } r>R\\ 0 & \text{if } r<R,\end{cases} \tag{A12b}$$

$$B_z=\begin{cases}0 & \text{if } r>R\\ \mu_0 I/a & \text{if } r<R.\end{cases} \tag{A12c}$$

These solutions are the same as those obtained by approximating the solenoid as a cylindrical current sheet. Note that there is an often-neglected external field arising from the (usually small) axial component of the current.

c. Solution for n≠0

To solve Eqs. (A11) for $n\neq 0$, we introduce a dimensionless radial variable ρ,

$$\rho(n,r)\equiv 2\pi nr/a \quad \text{with} \quad \rho_0\equiv\rho(n,R)=2\pi nR/a. \tag{A13}$$

For convenience, we suppress the dependence of the $b_{i,n}$ on n and r, i.e., where b_i appears below, read $b_{i,n}(\rho)$.

If Eq. (A11b) is used to eliminate b_ϕ from Eq. (A11d), Eq. (A11c) is reproduced. Thus, we have only three independent equations to solve,

$$\frac{1}{\rho}b_r+\frac{db_r}{d\rho}+\frac{in}{\rho}b_\phi-ib_z=0, \tag{A14a}$$

$$b_\phi=-\frac{n}{\rho}b_z, \tag{A14b}$$

$$-ib_r-\frac{db_z}{d\rho}=\frac{\mu_0 I}{2\pi n}\delta(r-R)\exp\left(\frac{i2\pi nz_0}{a}\right). \tag{A14c}$$

Using Eq. (A14b) to eliminate b_ϕ from Eq. (A14a) gives

$$\frac{1}{\rho}b_r+\frac{db_r}{d\rho}-i\left(1+\frac{n^2}{\rho^2}\right)b_z=0. \tag{A15}$$

For $r\neq R$, Eq. (A14c) becomes

$$-ib_r-db_z/d\rho=0. \tag{A16}$$

Using this to eliminate b_r from Eq. (A15) we obtain the modified Bessel equation

$$\frac{d^2b_z}{d\rho^2}+\frac{1}{\rho}\frac{db_z}{d\rho}-\left(1+\frac{n^2}{\rho^2}\right)b_z=0, \tag{A17}$$

which has solutions $I_n(\rho)$ and $K_n(\rho)$ [43]. The general solution is therefore

$$b_{z,n}(\rho)=\alpha I_n(\rho)+\beta K_n(\rho). \tag{A18}$$

The asymptotic behavior of the modified Bessel functions as $\rho\to\infty$ is

$$I_n(\rho)\simeq\frac{1}{\sqrt{2\pi\rho}}\exp(\rho),\quad K_n(\rho)\simeq\sqrt{\frac{\pi}{2\rho}}\exp(-\rho), \tag{A19}$$

and as $\rho\to 0$

$$I_n(\rho)\simeq\frac{1}{n!}\left(\frac{\rho}{2}\right)^n,\quad K_n(\rho)\simeq\frac{(n-1)!}{2}\left(\frac{2}{\rho}\right)^n. \tag{A20}$$

Since b_z must remain finite as $\rho\to 0$ and as $\rho\to\infty$, this restricts the solutions to

$$b_z=\begin{cases}\beta K_n(\rho) & \text{if } \rho>\rho_0\\ \alpha I_n(\rho) & \text{if } \rho<\rho_0.\end{cases} \tag{A21}$$

From Eqs. (A14b) and (A16) we find

$$b_\phi=\begin{cases}-(\beta n/\rho)K_n(\rho) & \text{if } \rho>\rho_0\\ -(\alpha n/\rho)I_n(\rho) & \text{if } \rho<\rho_0,\end{cases} \tag{A22}$$

$$b_r=\begin{cases}\beta i K_n'(\rho) & \text{if } \rho>\rho_0\\ \alpha i I_n'(\rho) & \text{if } \rho<\rho_0.\end{cases} \tag{A23}$$

Here and below, the prime ($'$) indicates differentiation with respect to ρ.

Integrating Eqs. (A14c) and (A15) from $\rho_0-\epsilon$ to $\rho_0+\epsilon$, where ϵ is an infinitessimal positive number, we find

$$\alpha I_n(\rho_0)-\beta K_n(\rho_0)=\frac{\mu_0 I}{a}\exp\left(\frac{i2\pi nz_0}{a}\right), \tag{A24a}$$

$$\alpha I_n'(\rho_0)=\beta K_n'(\rho_0). \tag{A24b}$$

Equation (A24b) is satisfied trivially if we put

$$\alpha=\gamma K_n'(\rho_0),\quad \beta=\gamma I_n'(\rho_0), \tag{A25}$$

where γ is another constant. From Eq. (A24a) we obtain

$$\gamma\{I_n(\rho_0)K_n'(\rho_0)-K_n(\rho_0)I_n'(\rho_0)\}=(\mu_0 I/a)\exp\left(\frac{i2\pi nz_0}{a}\right). \tag{A26}$$

The expression in braces is the Wronskian of the modified Bessel functions, equal to $-1/\rho_0$. Therefore

$$\gamma=-(\mu_0 I\rho_0/a)\exp\left(\frac{i2\pi nz_0}{a}\right). \tag{A27}$$

Thus, the solution for $n\neq 0$ is

$$b_r=-\frac{i\mu_0 I\rho_0}{a}\exp\left(\frac{i2\pi nz_0}{a}\right)\times\begin{cases}I_n'(\rho_0)K_n'(\rho) & \text{if } \rho>\rho_0\\ K_n'(\rho_0)I_n'(\rho) & \text{if } \rho<\rho_0,\end{cases} \tag{A28a}$$

$$b_\phi=\frac{\mu_0 In\rho_0}{a\rho}\exp\left(\frac{i2\pi nz_0}{a}\right)\times\begin{cases}I_n'(\rho_0)K_n(\rho) & \text{if } \rho>\rho_0\\ K_n'(\rho_0)I_n(\rho) & \text{if } \rho<\rho_0,\end{cases} \tag{A28b}$$

$$b_z=-\frac{\mu_0 I\rho_0}{a}\exp\left(\frac{i2\pi nz_0}{a}\right)\times\begin{cases}I_n'(\rho_0)K_n(\rho) & \text{if } \rho>\rho_0\\ K_n'(\rho_0)I_n(\rho) & \text{if } \rho<\rho_0.\end{cases} \tag{A28c}$$

d. Summary

Combining the results for $n=0$ and $n\neq 0$, we obtain For $r>R$

$$B_r=\frac{\mu_0 I4\pi R}{a^2}\sum_{n=1}^{\infty}n\sin\left[n\left(\phi-\frac{2\pi}{a}(z-z_0)\right)\right]\times I_n'\left(\frac{2\pi nR}{a}\right)K_n'\left(\frac{2\pi nr}{a}\right), \tag{A29a}$$

$$B_\phi=\frac{\mu_0 I}{2\pi r}+\frac{\mu_0 I 2R}{ar}\sum_{n=1}^{\infty} n\cos\left[n\left(\phi-\frac{2\pi}{a}(z-z_0)\right)\right]$$
$$\times I_n{}'\left(\frac{2\pi nR}{a}\right)K_n\left(\frac{2\pi nr}{a}\right), \quad \text{(A29b)}$$

$$B_z=-\frac{\mu_0 I 4\pi R}{a^2}\sum_{n=1}^{\infty} n\cos\left[n\left(\phi-\frac{2\pi}{a}(z-z_0)\right)\right]$$
$$\times I_n{}'\left(\frac{2\pi nR}{a}\right)K_n\left(\frac{2\pi nr}{a}\right), \quad \text{(A29c)}$$

and for $r<R$

$$B_r=\frac{\mu_0 I 4\pi R}{a^2}\sum_{n=1}^{\infty} n\sin\left[n\left(\phi-\frac{2\pi}{a}(z-z_0)\right)\right]$$
$$\times K_n{}'\left(\frac{2\pi nR}{a}\right)I_n{}'\left(\frac{2\pi nr}{a}\right), \quad \text{(A30a)}$$

$$B_\phi=\frac{\mu_0 I 2R}{ar}\sum_{n=1}^{\infty} n\cos\left[n\left(\phi-\frac{2\pi}{a}(z-z_0)\right)\right]$$
$$\times K_n{}'\left(\frac{2\pi nR}{a}\right)I_n\left(\frac{2\pi nr}{a}\right), \quad \text{(A30b)}$$

$$B_z=\frac{\mu_0 I}{a}-\frac{\mu_0 I 4\pi R}{a^2}\sum_{n=1}^{\infty} n\cos\left[n\left(\phi-\frac{2\pi}{a}(z-z_0)\right)\right]$$
$$\times K_n{}'\left(\frac{2\pi nR}{a}\right)I_n\left(\frac{2\pi nr}{a}\right). \quad \text{(A30c)}$$

e. The axial magnetic field

We examine the magnetic field on axis ($r=0$). The only nonzero terms in Eqs. (A30) are the $n=0$ and $n=1$ terms. We find

$$B_r=\frac{\mu_0 I 2\pi R}{a^2}\sin\left(\phi-\frac{2\pi}{a}(z-z_0)\right)K_1{}'\left(\frac{2\pi R}{a}\right), \quad \text{(A31a)}$$

$$B_\phi=\frac{\mu_0 I 2\pi R}{a^2}\cos\left(\phi-\frac{2\pi}{a}(z-z_0)\right)K_1{}'\left(\frac{2\pi R}{a}\right), \quad \text{(A31b)}$$

$$B_z=\frac{\mu_0 I}{a}. \quad \text{(A31c)}$$

The corresponding cartesian components are

$$B_x=-\frac{\mu_0 I 2\pi R}{a^2}\sin\left(\frac{2\pi}{a}(z-z_0)\right)K_1{}'\left(\frac{2\pi R}{a}\right), \quad \text{(A32a)}$$

$$B_y=\frac{\mu_0 I 2\pi R}{a^2}\cos\left(\frac{2\pi}{a}(z-z_0)\right)K_1{}'\left(\frac{2\pi R}{a}\right), \quad \text{(A32b)}$$

$$B_z=\frac{\mu_0 I}{a}. \quad \text{(A32c)}$$

This field has a nonzero component perpendicular to the axis, and makes one complete revolution over distance a in the z direction. The magnitude of this component is

$$|\boldsymbol{B}_\perp|=\sqrt{B_x^2+B_y^2}=\frac{\mu_0 I 2\pi R}{a^2}K_1{}'\left(\frac{2\pi R}{a}\right). \quad \text{(A33)}$$

Using the dimensions of our guide, the relative magnitudes of the perpendicular and axial field components are $|B_\perp/B_z|\sim 10^{-4}$, so the small perpendicular field component can be neglected for many purposes.

4. The double wound solenoid

A double-wound solenoid consists of two single-wire solenoids interwound, each of periodicity a. One coil carries current I and has $z_0=0$; the other $-I$ and $z_0=a/2$. Using the single-solenoid results, we find the magnetic field $\boldsymbol{B}$ of the double-wound solenoid.

For $r>R$

$$B_r=\frac{\mu_0 I 8\pi R}{a^2}\sum_{n=0}^{\infty}(2n+1)\sin\left[(2n+1)\left(\phi-\frac{2\pi z}{a}\right)\right]$$
$$\times I_{2n+1}{}'\left((2n+1)\frac{2\pi R}{a}\right)K_{2n+1}{}'\left((2n+1)\frac{2\pi r}{a}\right), \quad \text{(A34a)}$$

$$B_\phi=\frac{\mu_0 I 4R}{ar}\sum_{n=0}^{\infty}(2n+1)\cos\left[(2n+1)\left(\phi-\frac{2\pi z}{a}\right)\right]$$
$$\times I_{2n+1}{}'\left((2n+1)\frac{2\pi R}{a}\right)K_{2n+1}\left((2n+1)\frac{2\pi r}{a}\right), \quad \text{(A34b)}$$

$$B_z = -\frac{\mu_0 I 8\pi R}{a^2}\sum_{n=0}^{\infty}(2n+1)\cos\left[(2n+1)\left(\phi-\frac{2\pi z}{a}\right)\right]\times I_{2n+1}{}'\left((2n+1)\frac{2\pi R}{a}\right)K_{2n+1}\left((2n+1)\frac{2\pi r}{a}\right), \tag{A34c}$$

and for $r<R$

$$B_r = \frac{\mu_0 I 8\pi R}{a^2}\sum_{n=0}^{\infty}(2n+1)\sin\left[(2n+1)\left(\phi-\frac{2\pi z}{a}\right)\right]\times K_{2n+1}{}'\left((2n+1)\frac{2\pi R}{a}\right)I_{2n+1}{}'\left((2n+1)\frac{2\pi r}{a}\right), \tag{A35a}$$

$$B_\phi = \frac{\mu_0 I 4R}{ar}\sum_{n=0}^{\infty}(2n+1)\cos\left[(2n+1)\left(\phi-\frac{2\pi z}{a}\right)\right]\times K_{2n+1}{}'\left((2n+1)\frac{2\pi R}{a}\right)I_{2n+1}\left((2n+1)\frac{2\pi r}{a}\right), \tag{A35b}$$

$$B_z = -\frac{\mu_0 I 8\pi R}{a^2}\sum_{n=0}^{\infty}(2n+1)\cos\left[(2n+1)\left(\phi-\frac{2\pi z}{a}\right)\right]\times K_{2n+1}{}'\left((2n+1)\frac{2\pi R}{a}\right)I_{2n+1}\left((2n+1)\frac{2\pi r}{a}\right). \tag{A35c}$$

On the axis of the double-wound solenoid, the axial component of the magnetic field is zero, but there is still a component of the field perpendicular to the z direction, with magnitude twice that of the single solenoid.

[1] H. J. Metcalf and P. van der Straten, *Laser Cooling and Trapping* (Springer, New York, 1999).
[2] V. I. Balykin, V. G. Minogin, and V. S. Letokhov, Rep. Prog. Phys. **63**, 1429 (2000).
[3] *Atom Interferometry*, edited by P. Berman (Academic Press, San Diego, 1997).
[4] M. H. Anderson, J. R. Ensher, M. R. Matthews, C. E. Wieman, and E. A. Cornell, Science **269**, 198 (1995).
[5] K. B. Davis, M-O. Mewes, M. R. Andrews, N. J. van Druten, D. S. Durfee, D. M. Kurn, and W. Ketterle, Phys. Rev. Lett. **75**, 1687 (1995).
[6] M-O. Mewes, M. R. Andrews, D. M. Kurn, D. S. Durfee, C. G. Townsend, and W. Ketterle, Phys. Rev. Lett. **78**, 582 (1997).
[7] B. P. Anderson and M. A. Kasevich, Science **282**, 1686 (1998).
[8] E. W. Hagley, L. Deng, M. Kozuma, J. Wen, K. Helmerson, S. I. Rolston, and W. D. Phillips, Science **283**, 1706 (1999).
[9] I. Bloch, T. W. Hänsch, and T. Esslinger, Phys. Rev. Lett. **82**, 3008 (1999).
[10] R. Grimm, M. Weidemüller, and V. R. Ovchinnikov, Adv. At., Mol., Opt. Phys. **42**, 95 (2000).
[11] I. H. Deutsch and P. S. Jessen, Phys. Rev. A **57**, 1972 (1998).
[12] D. Muller, E. A. Cornell, D. Z. Anderson, and E. R. Abraham, Phys. Rev. A **61**, 033411 (2000).
[13] R. G. Dall, M. D. Hoogerland, K. G. H. Baldwin, and S. J. Buckman, J. Opt. B: Quantum Semiclassical Opt. **1**, 396 (1999).
[14] H. Ito, K. Sakaki, M. Ohtsu, and W. Jhe, Appl. Phys. Lett. **70**, 2496 (1997).
[15] M. J. Renn, A. A. Zozulya, E. A. Donley, E. A. Cornell, and D. Z. Anderson, Phys. Rev. A **55**, 3684 (1997).
[16] K. Bongs, S. Burger, S. Dettmer, D. Hellweg, J. Arlt, W. Ertmer, and K. Sengstock, Phys. Rev. A **63**, 031602 (2001).
[17] X. Xu, K. Kim, and W. Jhe, J. Korean Phys. Soc. **37**, 661 (2000).
[18] Min Yan, Yifu Zhu, and Jiangpin Yin, J. Opt. Soc. Am. B **17**, 1817 (2000).
[19] J. Arlt and K. Dholakia, Opt. Commun. **177**, 297 (2000).
[20] Y. Song, D. Milam, and W. T. Hill III, Opt. Lett. **24**, 1805 (1999).
[21] L. Pruvost, D. Marescaux, O. Houde, and Hong Tuan Duong, Opt. Commun. **166**, 199 (1999).
[22] G. Birkl, F. B. J. Buchkremer, R. Dumke, and W. Ertmer, Opt. Commun. **191**, 67 (2001).
[23] A. H. Barnett, S. P. Smith, M. Olshanii, K. S. Johnson, A. W. Adams, and M. Prentiss, Phys. Rev. A **61**, 023608 (2000).
[24] E. A. Hinds and I. G. Hughes, J. Phys. D **32**, R119 (1999).
[25] A. Goepfert, P. Lison, R. Schutze, R. Wynands, D. Haubrich, and D. Meschede, Appl. Phys. B: Lasers Opt. **69**, 217 (1999).
[26] D. Meschede, I. Bloch, A. Goepfert, D. Haubrich, M. Kreis, F. Lison, R. Schutze, and R. Wynands, Proc. SPIE **2995**, 191 (1997).
[27] J. Denschlag, D. Cassettari, and J. Schmiedmayer, Phys. Rev. Lett. **82**, 2014 (1999).
[28] J. Fortagh, H. Ott, A. Grossman, and C. Zimmermann, Appl. Phys. B: Lasers Opt. **70**, 701 (2000).
[29] B. K. Teo and G. Raithel, Phys. Rev. A **63**, 031402 (2001).
[30] M. Key, I. G. Hughes, W. Rooijakkers, B. E. Sauer, E. A. Hinds, D. J. Richardson, and P. G. Kazansky, Phys. Rev. Lett. **84**, 1371 (2000).
[31] E. A. Hinds, C. J. Vale, and M. G. Boshier, Phys. Rev. Lett. **86**, 1462 (2001).
[32] L. Xu, J. Yin, and Y. Wang, Opt. Commun. **188**, 93 (2001).
[33] J. A. Richmond, S. Nic Chormaic, B. P. Cantwell, and G. I. Opat, Acta Phys. Slov. **48**, 481 (1998).
[34] K. Brugger, T. Calarco, D. Cassettari, R. Folman, A. Haase, B. Hessmo, P. Kruger, T. Maier, and J. Schmiedmayer, J. Mod. Opt. **47**, 2789 (2000).
[35] K. I. Lee, J. A. Kim, H. R. Noh, and W. Jhe, Opt. Lett. **21**, 1177 (1996).

[36] J. Reichel, W. Hänsel, and T. W. Hänsch, Phys. Rev. Lett. **83**, 3398 (1999).
[37] N. H. Dekker, C. S. Lee, V. Lorent, J. H. Thywissen, S. P. Smith, M. Drndic, R. M. Westervelt, and M. Prentiss, Phys. Rev. Lett. **84**, 1124 (2000).
[38] R. Folman, P. Krüger, D. Cassettari, B. Hessmo, T. Maier, and J. Schmiedmayer, Phys. Rev. Lett. **84**, 4749 (2000).
[39] D. Cassettari, B. Hessmo, R. Folman, T. Maier, and J. Schmiedmayer, Phys. Rev. Lett. **85**, 5483 (2000).
[40] J. Reichel, W. Hänsel, P. Hommelhoff, and T. W. Hänsch, Appl. Phys. B: Lasers Opt. **72**, 81 (2001).
[41] D. Muller, E. A. Cornell, M. Prevedelli, P. D. D. Schwindt, Y. J. Wang, and D. Z. Anderson, Phys. Rev. A **63**, 041602 (2001).
[42] D. Halliday, R. Resnick, and J. Walker, *Fundamentals of Physics*, 6th ed. (Wiley, New York, 2001), p. 698.
[43] *Handbook of Mathematical Functions with Formulas, Graphs and Mathematical Tables*, edited by M. Abramowitz and I. A. Stegun (Dover, New York, 1965), p. 374.